Geological Magazine

www.cambridge.org/geo

Original Article

Cite this article: Nawrocki J, Pańczyk M, and Szrek P (2020) Magmatic activity at the Silurian/Devonian boundary in the Brunovistulia and Małopolska Terranes (S Poland): possible link with the Rheic Ocean closure and the onset of the Rheno-Hercynian Basin. *Geological Magazine* **157**: 119–133. https://doi.org/10.1017/S0016756819000384

Received: 17 October 2017
Revised: 29 March 2019
Accepted: 2 April 2019
First published online: 17 May 2019

Keywords:
mafic-intermediate intrusions; tuffs; U–Pb ages; extension

Author for correspondence: Jerzy Nawrocki, Email: jerzy.nawrocki@poczta.umcs.lublin.pl

Magmatic activity at the Silurian/Devonian boundary in the Brunovistulia and Małopolska Terranes (S Poland): possible link with the Rheic Ocean closure and the onset of the Rheno-Hercynian Basin

Jerzy Nawrocki[1], Magdalena Pańczyk[2] and Piotr Szrek[2]

[1]Faculty of Earth Sciences and Spatial Management, Maria Curie-Skłodowska University, Al. Kraśnicka 2cd, 20-718 Lublin, Poland and [2]Polish Geological Institute – National Research Institute, Rakowiecka 4, 00-975 Warsaw, Poland

Abstract

The age of granophyric diorite from the Sosnowiec IG-1 borehole (Brunovistulia Terrane) was studied by means of U–Pb single-grain zircon analysis performed on a SHRIMP (sensitive high-resolution ion microprobe) IIe device. The isotope ages and provenance of zircons from the Emsian tuffs cropping out in the southern part of the Holy Cross Mountains (Małopolska Terrane) were also investigated using the same method. The age of the diorite intrusion (420 ± 2 Ma) is comparable with the combined Ar–Ar/magnetostratigraphic age of the Bardo diabase intrusion from the northern part of the Małopolska Terrane. These intrusions were emplaced during the same event of regional tectonic extension associated with the Rheic Ocean closure and the onset of processes creating the Rheno-Hecynian Basin near the Silurian/Devonian boundary. A negative Nb anomaly characteristic of both intrusions could be linked with the subduction of the Rheic oceanic crust under the SE margin of the Old Red Continent. Emsian magmatic activity in the distant Rheno-Hercynian Zone provided several tuff layers in the northern part of the Małopolska Terrane. As can be inferred from zircon ages, these tuffs were derived from mafic eruptions that cut sedimentary rocks containing detrital zircons transported from Baltica. This interpretation fits the existing models of development of the Rheno-Hercynian Basin in the Emsian.

1. Introduction

The latest stages of the Caledonian and the earliest stages of Variscan orogenic cycles that affected the marginal zone of the Old Red Continent in southern Poland are still unsatisfactorily recognized. In some places they are expressed by a tectonic discordance (Kowalczewski & Lisik, 1974; Buła, 2000), coarse-grained deposits along the major fault zones (Buła, 2000; Malec, 2001) and magmatic bodies (Nawrocki *et al.* 2013). This area consists of two tectonostratigraphic units, the Małopolska Terrane (MT) and the neighbouring Brunovistulian Terrane (BVT) (e.g. Dudek, 1980; Belka *et al.* 2002; Żelaźniewicz *et al.* 2009). Several magmatic bodies were penetrated by the boreholes located in the border area of both units defined by the NW-trending, crustal-scale Kraków–Lubliniec Fault Zone (e.g. Żaba, 1999; Malinowski *et al.* 2005). Mafic intrusions were also drilled by the deep borehole of Goczałkowice IG-1 and Sosnowiec IG-1, located *c.* 50 km from this zone (Fig. 1a). However, the poor age constraints on the pre-late Carboniferous magmatic activity in the area of the BVT make the relationship of these processes with the tectonic evolution of Central Europe unclear.

The aim of this paper is to provide a reliable and accurate age of prominent diorite intrusion from the BVT drilled in the Sosnowiec IG-1 borehole, using U–Pb zircon single grain dating. The next aim is to ascertain if this intrusion and another extensive mafic intrusion from the Bardo syncline in the MT were emplaced during approximately the same extensional event at the turn of Silurian and Devonian. Both intrusions have a distinct signature of anorogenic magmatics, typical of continental extensional settings (Krzemiński, 2004).

Additionally, we examined ages of zircons derived from the early Emsian tuffs cropping out among Emsian clastic rocks in the southern region of the Holy Cross Mountains, in order to define the source of tuffs and zircons, and to check whether they fit with existing knowledge about the early Devonian palaeogeography of neighbouring areas. Finally, we attempt to link the studied magmatic activity with continental-scale processes operating at the margin of the Old Red Continent at the transition from the Caledonian to Variscan cycle.

2. Geological setting

The BVT, comprising the Upper Silesian Block, is a complex terrane that was consolidated in the Neoproterozoic (e.g. Dudek, 1980; Żelaźniewicz *et al.* 2009). Palaeozoic rocks of the BVT in the Kraków–Lubliniec Fault Zone were disturbed by strike-slip motions during two periods: firstly at the end of the Silurian (sinistral transpression) and later during the late Carboniferous (dextral transpression and transtension) (Bogacz & Krokowski, 1981; Żaba, 1999). Winchester *et al.* (2002) have defined the MT as a Neoproterozoic accretionary prism of the BVT and pointed out that both terranes were always close to each other and the Baltica palaeocontinent. In fact, the lithostratigraphic and structural records on both sides of the KLFZ became similar from the Emsian (Buła, 2000). The Emsian cover of the 'old red' type deposits may indicate that final amalgamation of the BVT took place sometime between the Silurian and Devonian (e.g. Dadlez, 1995; Belka *et al.* 2002; Nawrocki *et al.* 2004). The proximity of the BVT and MT since the Emsian can be inferred from the distribution of particular 'old red' facies (Pajchlowa & Miłaczewski, 1974). An argument for a substantially older spatial linkage of both terranes arises from their Cambrian trilobite faunas. The trilobite *Schmidiellus panowi* (Samsonowicz) found in the Cambrian sediments of the Holy Cross Mountains (belonging to the MT) and Upper Silesia is endemic at the species level to both areas (Żylińska, 2002; Nawrocki *et al.* 2004), and at the genus level points to a link with Baltica (Żylińska, 2002). Many authors postulate a peri-Gondwana origin of the BVT, hence its link with the South American (Hegner & Kröner, 2000; Friedl *et al.* 2001; Belka *et al.* 2002; Mazur *et al.* 2010; Walczak & Bełka, 2017) or African part of the peri-Gondwana orogenic belt (Unrug *et al.* 1999; Leichman & Höck, 2001). Moczydłowska (1997) has defined the BVT as part of East Avalonia. On the other hand, some authors postulate a peri-Baltic initial location of the BVT, i.e. near the Uralian margin of this palaeocontinent (Fatka & Vavrdova, 1998) or close to its southern present-day edge that was also involved in the Neoproterozoic peri-Gondwana orogen (Winchester *et al.* 2002; Nawrocki *et al.* 2004). The MT is defined by most authors as always linked with the Baltica foreland (e.g. Dadlez, 1995; Nawrocki & Poprawa, 2006; Żelaźniewicz *et al.* 2009) or peri-Gondwana that collided with Baltica in the early Palaeozoic before the collision with Avalonia (Belka *et al.* 2002; Walczak & Bełka, 2017). Palaeomagnetic data (Nawrocki, 2000; Shatz *et al.* 2006) suggest that large-scale wandering of the MT, if it occurred, must have ended before the Late Ordovician. During the Variscan orogeny, the BVT represented the lower plate of the southern margin of the Old Red Continent, involved in the collision with the Armorican Terrane Assemblage (e.g. Kalvoda *et al.* 2008).

Along the boundary between the BVT and MT, several late Carboniferous – early Permian magmatic bodies have been penetrated by boreholes (e.g. Buła, 2000; Żelaźniewicz *et al.* 2008; Nawrocki *et al.* 2010; Słaby *et al.* 2010). Mafic intrusions have also been drilled in the area of the BVT *c.* 50 km from the KLFZ. A diabase–diorite polycyclic intrusion of *c.* 90 m thickness, drilled here in the Sosnowiec IG-1 borehole, cuts Middle Cambrian clastic rocks. Samples from the dioritic parts of this intrusion gave a ^{40}Ar–^{39}Ar plateau age of 399.4 ± 1.8 Ma, obtained on an amphibole concentrate, but the whole-rock ^{40}Ar–^{39}Ar dating of the diabase part of the same intrusion revealed a plateau age of 289.1 ± 1.8 Ma (Nawrocki *et al.* 2010).

The most extensive mafic intrusion recognized in the area of the MT fills the Bardo Syncline in the Kielce Region of the Holy Cross Mountains. (Fig. 1a, b). This diabase is up to 30 m thick and penetrates Silurian rocks of the syncline, close to the stratigraphic boundary between Gorstian graptolite shales and Ludfordian greywackes (Kowalczewski & Lisik, 1974). A relatively precise age of the Bardo intrusion was inferred from the comparison of the ^{40}Ar–^{39}Ar isotope dating and the normal polarity palaeomagnetic record that was correlated with the global polarity timescale (Nawrocki *et al.* 2013). According to these data, the intrusion was formed in the age interval between 425 and 417 Ma, preceding the late Lochkovian tectonic event expressed in the Holy Cross Mountains by the Gruchawka Conglomerates, and the tectonic unconformity observed in the Bardo Syncline where the Silurian strata were more intensively folded than the overlying Emsian sandstones (Kowalczewski & Lisik, 1974; Malec, 2001).

Silurian (438 ± 16 Ma) magmatic activity has been documented through K–Ar dating of a basalt vein intruding into the Brunovistulian basement in Moravia (Přichystal, 1999). S Hoenig (unpub. PhD thesis, Masaryk Univ., Brno, 2016) links the extensional anorogenic magmatism recognized in this part of the BVT with the Silurian subduction. The magmatic activity or metamorphism of Silurian age is also supported by common occurrences of Silurian micas and monazites in Carboniferous sedimentary sequences (Kusiak *et al.* 2006). The Quenast quartz–diorite from the Brabant Massif *c.* 430 Ma old (Linnemann *et al.* 2012) might be regarded as a distant correlative.

3. Material and methods

One sample for U–Pb dating of zircon grains was collected from massive, granophyric diorite drilled in the Sosnowiec IG-1 borehole (Fig. 2; sample depth 3259.5 m) which comprises mostly altered plagioclases and amphiboles affected by chloritization (Krzemiński, 2004; Nawrocki *et al.* 2010). These pyroxene and amphibole diorite samples on the Zr/TiO_2 – Nb/Y classification diagram plot within the basaltic-andesite field and have a high Fe/Mg ratio and silica content indicating a tholeiitic affinity (Krzemiński, 2004).

Four samples for U–Pb dating of detrital zircon grains were taken from the Emsian tuffs of the Holy Cross Mountains. These tuffs were sampled in the Podłazie and Ujazd sections (Figs 2, 3a, b). Based on miospores and tephro-correlation, the succession from Podłazie is considered to be Emsian in age (Tarnowska, 1976; Szulczewski & Porębski, 2008), and belongs to the lower part of the Winna Formation (see Fijałkowska-Mader & Malec, 2011). The section is composed of sandstones, mudstones and tuffs. The light-grey, strongly altered tuffs can exceed 15 cm in thickness. The second studied section, Ujazd near Iwaniska, is located in the same Kielce Region of the Holy Cross Mountains. This section is composed of sandstones interbedded with light-grey, strongly altered tuffs (up to 20 cm thick). In this locality some poorly preserved vertebrate remains were found. They represent sarcopterygians and placoderms corresponding to the assemblage from the Podłazie locality (Szrek & Dupret, 2017). This suggests the similar stratigraphic position of this section. Bearing in mind the Emsian age of the whole Winna Formation (see e.g. Wójcik, 2015), we assume that the age of the studied section should correspond approximately to 405 Ma (see Gradstein *et al.* 2012). The strongly altered tuffs (bentonites) from both sections are composed of former glassy ash, single crystals of quartz, rock fragments of volcanic origin (presumably scoriae) as well as opaque minerals and zircon grains (Fig. 3c–f). The clasts of volcanogenic rocks are strongly altered and compacted without

https://doi.org/10.1017/S0016756819000384 Published online by Cambridge University Press

Fig. 1. (a) The location of sites for U–Pb age estimation on a terrane map of Poland (see Nawrocki, 2015) (CDF – Caledonian Deformation Front; LTT – Teisseyre–Tornquist tectonic line; GF – Grójec Fault; DFZ – Dolsk Fault Zone; OF – Odra Fault; KLFZ – Kraków–Lubliniec Fault Zone; MTL – Moravian Tectonic Line; HCF – Holy Cross Fault; SD – Sosnowiec IG-1 borehole with diorite intrusion; BD – Bardo diabase; LC – Łapczyca conglomerate; MC – Miedziana Góra conglomerate; GC – Gruchawka conglomerate; P – Podłazie; U – Ujazd). (b) Main palaeotectonic regions of the Palaeozoic core of the Holy Cross Mountains (Czarnocki, 1938).

any phenocrysts of quartz and other minerals. The altered glass shards and fragments of volcanogenic rocks consist of kaolinite, illite and other phyllosilicate minerals. Because of extensive alteration processes, the phenocrysts or phenoclasts of mafic minerals such as olivine and pyroxene are not observed. Additional particles of epiclastic origin, including small grains of quartz and fragments of claystones, are also rarely observed. Amygdales are filled by quartz and feldspar.

A sample of subvolcanic rock from the Sosnowiec IG-1 borehole (named: S) and four samples of tuffs from Podłazie (named: Pod-10, Pod-26, Pod- 30) and Ujazd (named: U-6) were crushed and sieved for zircon separation. Heavy mineral fractions were separated using conventional heavy-liquid and magnetic techniques. All hand-picked zircons from the studied samples, and several grains of the TEMORA standard and two grains of the SL13 zircons standard were cast into an epoxy mount. These were polished and observed using an optical microscope (reflected and transmitted light), then imaged by cathodoluminescence (CL) using a Hitachi SU3500 scanning electron microscope (SEM) for evaluation of the zircons from the Sosnowiec subvolcanic rocks and a Zaiss EVO 10 SEM for zircons separated from tuffs. The CL images were used to characterize the zircon grains and select locations for isotope analyses. The sample from the Sosnowiec IG-1 borehole was analysed using a SHRIMP IIe/MC ion microprobe in the Micro-area Analysis Laboratory of the Polish Geological Institute – NRI, whereas the zircons separated from the tuffs were analysed using a SHRIMP IIe/MC ion microprobe at the IBERSIMS Lab (University of Granada, Spain). The analytical procedures for both instruments were based on those described by Williams & Claesson (1987).

Analytical conditions used for investigation of the sample were as follow: 3 nA negative O^{2-} primary ion beam focused to *c.* 25 µm diameter spot; mass resolution *c.* 5500; isotope ratio measurement by single electron multiplier and cyclic peak stepping. The selected spots were analysed over seven scans ($^{196}Zr_2O$ – 2 s; ^{204}Pb – 10 s; $^{204.1}$background – 10 s; ^{206}Pb – 15 s; ^{207}Pb – 20 s; ^{208}Pb – 15 s; ^{238}U – 10 s; ^{248}ThO – 5 s; ^{254}UO – 5 s). The TEMORA standard was measured every three spots. The data for the sample were reduced in a manner similar to that presented by Williams (1998, and references therein), using the SQUID Excel Macro of Ludwig (2000). Data reduction for the tuffs was done with the SHRIMPTOOLS software, specifically developed for IBERSIMS by F. Bea. Plots of SHRIMP results use ISOPLOT/EX (Ludwig, 2003) including a Tera–Wasserburg plot (Tera & Wasserburg, 1972) $^{238}U/^{206}Pb$ vs $^{207}Pb/^{206}Pb$ using data corrected for common Pb and probability density distribution plots for each sample. Ages were calculated

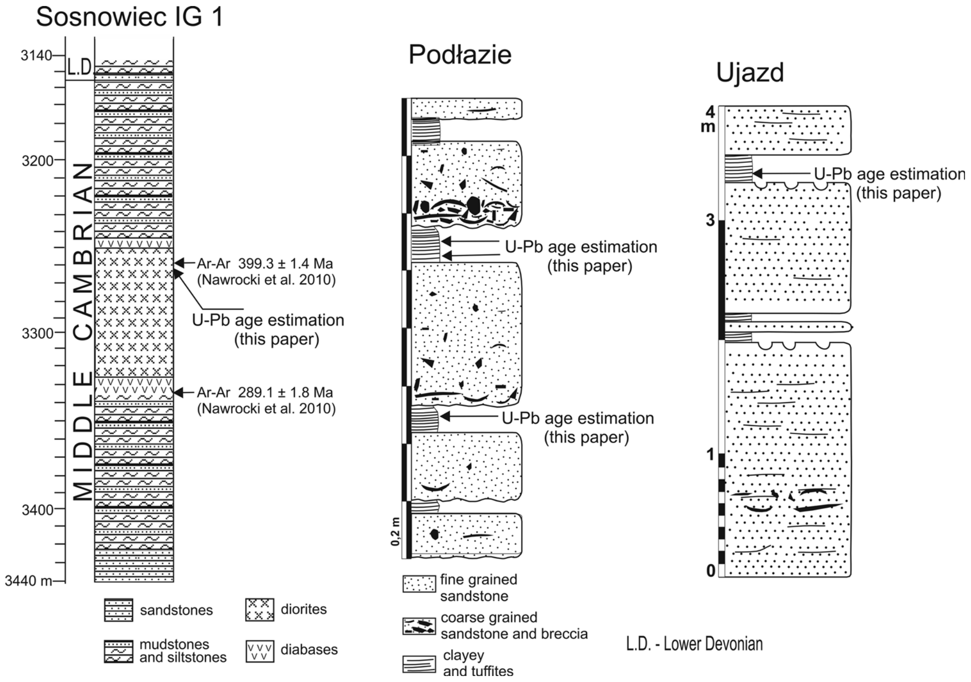

Fig. 2. Lithological columns of Middle Cambrian rocks drilled in the Sosnowiec IG-1 borehole and Emsian rocks cropping out in Podłazie and Ujazd with stratigraphic succession from the Holy Cross Mountains. Locations of samples for U–Pb age estimation of zircon grains are marked.

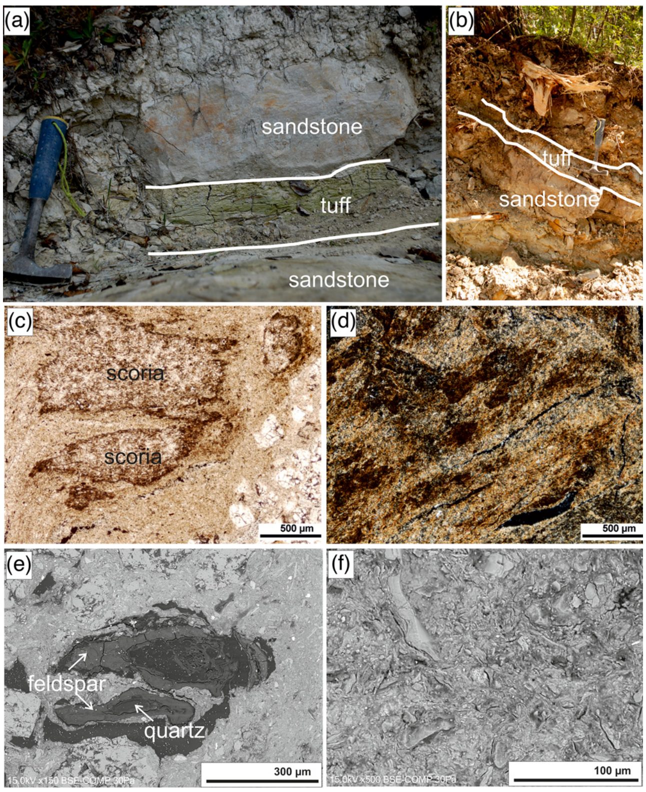

Fig. 3. (Colour online) (a) Sandstones interbedded with the light-grey, strongly altered tuffs in the Ujazd section. (b) The tuff layer in the Podłazie section. (c–f) Microphotographs of tuffs from Podłazie: volcanic clasts (scoria) surrounded by strongly altered ash (parallel polars) (c); strongly altered ash (crossed polars) (d); amygdaloids infilled by quartz and feldspar (backscatter electron image, BSE) (e); and strongly altered ash – mixture of kaolinite, illite and other phyllosilicate minerals and quartz (BSE) (f).

using the constants recommended by the International Union of Geological Sciences (IUGS) Subcommission on Geochronology (Steiger & Jäger, 1977).

4. Results of U–Pb dating

Results of our isotope studies are summarized in Tables 1 and 2. The zircon population from the Sosnowiec subvolcanic rocks is homogeneous and ranges from 80 to 120 µm in length. Almost all zircons are transparent and unzoned in CL images, with elongated prismatic crystals (Fig. 4a). Only two crystals from 37 separated grains are different: they are rounded, with evidence of dissolution and fragments of complicated zoning texture. The homogeneous, unzoned zircons from the Sosnowiec rocks have moderate U and Th contents (513–959 ppm and 373–1129 ppm, respectively) and typical Th/U ratio for igneous rocks, ranging from 0.74 up to 1.17. The SHRIMP results (Fig. 4b) are concordant and the calculated concordia age is 420 ± 2 Ma (mean square weighted deviation (MSWD) = 0.057, probability = 0.81, $n = 16$ after excluding zircons with discordance >10 and results with high error). Two inherited grains of zircon have lower Th/U ratios, 0.38 and 0.21, and lower concentrations of Th and U. These much older zircons provided ages of 1676 ± 16 and 970 ± 13 Ma (Table 1).

The zircons separated from the tuff samples are not homogeneous. Generally, they range from 50 to 150 µm in length. Most of them are transparent, pale-coloured and rounded (Fig. 5a). We were unable to identify a homogeneous subpopulation within any tuff samples. The CL images show a spectrum of textures including oscillatory as well as sector-zoning crystals with inherited cores and metamorphic grains with evidence of dissolution. Euhedral prismatic crystals with slightly rounded shapes occur rarely. The detrital zircons from the tuffs in both outcrops show

https://doi.org/10.1017/S0016756819000384 Published online by Cambridge University Press

https://doi.org/10.1017/S0016756819000384 Published online by Cambridge University Press

Table 1. Age estimation of zircon grains from the Sosnowiec diorite

Spot	U(ppm)	Th (ppm)	Th/U	^{206}Pb*(ppm)	^{204}Pb/^{206}Pb	±%	%^{206}Pbc	(1) ^{206}Pb/^{238}U Age		(1) ^{207}Pb/^{206}Pb Age		Total ^{238}U/^{206}Pb	±%	Total ^{207}Pb/^{206}Pb	±%	(1)^{238}U/^{206}Pb*	±%	(1) ^{207}Pb*/^{206}Pb*	±%
S.19.1	861	849	0.98527	48.6	−3.5E−5	44	–	410	±3	423	±18	15.22	0.64	0.05476	0.68	15.21	0.64	0.05527	0.79
S.9.1	890	1008	1.13297	50.7	1.3E−4	22	0.24	414	±3	374	±24	15.03	0.63	0.05602	0.66	15.07	0.63	0.05407	1.05
S.8.1	754	728	0.966403	43.1	7.2E−5	32	0.13	415	±8	369	±22	15.02	1.88	0.05502	0.71	15.04	1.88	0.05396	0.97
S.7.1	638	475	0.744658	36.7	−6.1E−5	39	–	418	±3	440	±22	14.96	0.67	0.05481	0.79	14.94	0.67	0.05570	0.99
S.26.1	910	1025	1.125804	52.4	6.4E−6	100	0.01	418	±2	450	±15	14.91	0.54	0.05604	0.65	14.91	0.54	0.05595	0.67
S.28.1	594	532	0.895289	34.3	−1.0E−4	33	–	419	±3	464	±27	14.90	0.70	0.05482	0.87	14.87	0.70	0.05628	1.21
S.5.1	838	724	0.864168	48.4	−6.7E−5	33	–	419	±3	440	±20	14.89	0.64	0.05471	0.70	14.87	0.64	0.05569	0.89
S.24.1	752	637	0.847198	43.6	−2.0E−5	65	–	421	±2	439	±18	14.84	0.54	0.05538	0.75	14.83	0.54	0.05567	0.82
S.6.1	709	630	0.888974	41.1	−8.0E−5	32	–	421	±3	475	±22	14.82	0.65	0.05541	0.74	14.80	0.65	0.05658	0.98
S.12.1	858	952	1.110314	49.9	5.4E−5	39	0.10	422	±7	395	±21	14.76	1.70	0.05536	0.75	14.78	1.70	0.05457	0.95
S.3.1	628	519	0.825743	36.6	–	–	0.00	422	±2	425	±18	14.77	0.55	0.05532	0.79	14.77	0.55	0.05532	0.79
S.2.1	815	854	1.047533	47.7	4.3E−6	134	0.01	425	±2	437	±16	14.68	0.54	0.05567	0.72	14.68	0.54	0.05561	0.73
S.16.1	903	906	1.002928	53.5	−6.3E−5	33	–	430	±5	455	±19	14.51	1.11	0.05514	0.68	14.49	1.11	0.05606	0.86
S.11.1	793	674	0.850463	47.1	−8.1E−6	100	–	431	±5	410	±17	14.45	1.19	0.05483	0.74	14.45	1.19	0.05494	0.77
S.23.1	948	1084	1.143466	57.3	−6.1E−6	106	–	439	±5	430	±16	14.20	1.10	0.05536	0.68	14.20	1.10	0.05545	0.70
S.14.1	118	26	0.218526	16.5	1.2E−4	58	0.21	970	±13	949	±42	6.15	1.45	0.07247	1.45	6.16	1.46	0.07072	2.07
S.25.1	129	50	0.389482	32.9	1.0E−5	100	0.02	1676	±16	1663	±12	3.37	1.10	0.10225	0.62	3.37	1.10	0.10211	0.64

Errors are 1-sigma; Pb_c and Pb* indicate the common and radiogenic portions, respectively.
Error in standard calibration was 0.15 % (not included in above errors but required when comparing data from different mounts).
(1) Common Pb corrected using measured ^{204}Pb.

https://doi.org/10.1017/S0016756819000384 Published online by Cambridge University Press

Table 2. Age estimation of detrital zircons from Podłazie and Ujazd

Spot	U (ppm)	Th (ppm)	Th/U	$^{206}Pb^{*}$ (ppm)	$^{204}Pb/^{206}Pb$	±err	f_{206_4} (%)	$^{206}Pb/^{238}U$ age	±err	$^{207}Pb/^{206}Pb$ age	±err	$^{207}Pb/^{206}Pb$	±err	$^{206}Pb/^{238}U$	±err
Pod-26-10.	119.5	55.4	0.48	24.4	−0.00004	0.00000	−0.1	1368.2	18.1	1390.3	8.4	0.08836	0.00039	0.23644	0.00346
Pod-26-11.	116.3	45.0	0.40	19.6	0.00000	0.00000	0.0	1148.2	18.3	1199.5	11.8	0.08010	0.00048	0.19496	0.00339
Pod-26-12.	161.4	70.1	0.45	32.2	0.00000	0.00000	0.0	1338.3	76.1	1328.5	72.6	0.08557	0.00329	0.23072	0.01444
Pod-26-13.	211.5	113.1	0.55	34.5	0.00001	0.00001	0.0	1114.6	7.3	1199.7	6.0	0.08011	0.00025	0.18875	0.00135
Pod-26-14.	73.1	21.8	0.31	13.5	0.00014	0.00005	0.2	1243.4	8.4	1207.1	4.8	0.08041	0.00020	0.21275	0.00159
Pod-26-16.	203.1	135.7	0.69	86.9	0.00003	0.00002	0.1	2589.3	9.4	2737.5	1.4	0.18947	0.00015	0.49431	0.00217
Pod-26-17.	166.2	107.6	0.66	44.3	0.00016	0.00001	0.3	1730.2	3.8	1783.5	6.6	0.10904	0.00039	0.30787	0.00078
Pod-26-18.	54.9	46.6	0.87	18.7	0.00003	0.00008	0.1	2139.8	5.7	2138.1	0.8	0.13301	0.00007	0.39366	0.00121
Pod-26-19.	143.2	156.5	1.12	31.9	0.00005	0.00002	0.1	1477.4	2.1	1492.9	0.8	0.09324	0.00004	0.25758	0.00042
Pod-26-19.	50.1	126.9	2.60	11.3	0.00030	0.00005	0.5	1496.0	61.6	1566.3	55.2	0.09696	0.00290	0.26120	0.01199
Pod-26-2.1	248.5	103.3	0.43	48.2	0.00006	0.00001	0.1	1302.6	5.1	1313.7	5.2	0.08492	0.00022	0.22394	0.00097
Pod-26-21.	136.4	68.1	0.51	18.8	0.00017	0.00010	0.3	950.5	7.0	992.7	5.6	0.07224	0.00020	0.15888	0.00127
Pod-26-22.	145.5	50.1	0.35	24.7	0.00010	0.00007	0.2	1155.4	2.5	1209.5	6.6	0.08051	0.00027	0.19630	0.00047
Pod-26-24.	81.3	33.8	0.43	11.2	0.00012	0.00014	0.2	954.1	7.2	970.3	29.0	0.07145	0.00103	0.15951	0.00130
Pod-26-27.	144.8	128.6	0.91	40.1	0.00001	0.00003	0.0	1788.7	17.0	1764.9	20.6	0.10793	0.00123	0.31979	0.00348
Pod-26-28.	111.6	60.8	0.56	27.6	0.00003	0.00006	0.1	1621.0	8.6	1609.9	7.4	0.09924	0.00039	0.28590	0.00172
Pod-26-3.1	184.4	66.9	0.37	30.4	0.00006	0.00000	0.1	1124.8	22.2	1122.5	34.2	0.07705	0.00134	0.19063	0.00410
Pod-26-30.	205.9	52.8	0.26	30.7	0.00005	0.00004	0.1	1022.9	7.7	1012.3	6.2	0.07294	0.00022	0.17196	0.00141
Pod-26-31.	141.9	54.8	0.40	28.3	0.00032	0.00003	0.6	1336.6	4.4	1388.9	9.2	0.08830	0.00042	0.23040	0.00084
Pod-26-32.	405.2	76.6	0.19	69.3	0.00000	0.00000	0.0	1162.7	3.9	1158.1	9.6	0.07844	0.00038	0.19765	0.00072
Pod-26-33.	194.0	116.6	0.62	11.7	0.00001	0.00019	0.0	435.8	0.9	470.1	1.0	0.05645	0.00003	0.06994	0.00016
Pod-26-34.	110.2	69.0	0.64	31.4	0.00005	0.00004	0.1	1834.2	9.9	1788.7	9.2	0.10936	0.00054	0.32915	0.00205
Pod-26-35.	204.3	145.4	0.73	58.2	0.00000	0.00000	0.0	1833.0	7.3	1850.7	2.2	0.11316	0.00014	0.32888	0.00151
Pod-26-36.	102.2	31.8	0.32	14.9	−0.00005	0.00005	−0.1	1003.5	20.3	975.5	12.0	0.07163	0.00042	0.16844	0.00368
Pod-26-37.	171.1	104.5	0.63	40.5	−0.00001	0.00004	0.0	1559.7	16.2	1570.1	6.0	0.09715	0.00031	0.27374	0.00321
Pod-26-38.	228.9	97.9	0.44	23.4	0.00000	0.00000	0.0	719.6	0.9	731.5	24.0	0.06369	0.00073	0.11809	0.00015
Pod-26-39.	107.4	120.5	1.15	23.7	0.00006	0.00010	0.1	1465.5	6.8	1489.1	7.2	0.09306	0.00035	0.25525	0.00133
Pod-26-39.	156.1	135.7	0.89	33.5	0.00009	0.00007	0.2	1426.7	6.8	1512.7	8.2	0.08334	0.00148	0.21042	0.00053
Pod-26-4.1	98.5	40.2	0.42	17.9	0.00000	0.00000	0.2	1231.0	2.8	1277.1	34.4	0.09514	0.00104	0.25226	0.00240
Pod-26-41.	51.6	61.3	1.22	11.3	0.00012	0.00004	0.0	1450.1	12.3	1530.9	20.4	0.09330	0.00144	0.25611	0.01226
Pod-26-41.	112.3	111.7	1.02	24.9	−0.00006	0.00006	0.2	1469.9	63.2	1493.9	29.0	0.07112	0.00038	0.17003	0.00161

(*Continued*)

https://doi.org/10.1017/S0016756819000384 Published online by Cambridge University Press

Table 2. (*Continued*)

Spot	U (ppm)	Th (ppm)	Th/U	$^{206}Pb^{*}$ (ppm)	$^{204}Pb/^{206}Pb$	±err	f_{206_4} (%)	$^{206}Pb/^{238}U$ age	±err	$^{207}Pb/^{206}Pb$ age	±err	$^{207}Pb/^{206}Pb$	±err	$^{206}Pb/^{238}U$	±err
Pod-26-42.	125.3	44.5	0.36	18.4	0.00002	0.00002	−0.1	1012.3	8.9	960.7	11.0	0.10195	0.00034	0.29270	0.00383
Pod-26-43.	261.6	115.0	0.45	66.3	−0.00008	0.00006	0.0	1655.0	19.1	1660.1	6.0	0.07854	0.00115	0.18675	0.00092
Pod-26-44.	50.9	15.1	0.30	8.2	0.00006	0.00004	−0.2	1103.7	5.0	1160.5	28.8	0.07746	0.00025	0.18805	0.00046
Pod-26-44.	317.6	97.1	0.31	51.7	0.00022	0.00007	0.1	1110.8	2.5	1132.9	6.4	0.05748	0.00061	0.06909	0.00115
Pod-26-5.1	168.3	115.5	0.70	10.1	0.00004	0.00003	0.4	430.7	6.9	509.9	23.4	0.09078	0.00075	0.24674	0.00039
Pod-26-6.1	159.3	120.9	0.78	34.0	0.00017	0.00007	0.1	1421.7	2.0	1441.9	15.8	0.07691	0.00246	0.15938	0.00463
Pod-26-8.1	96.1	51.8	0.55	26.0	0.00001	0.00006	0.0	1753.2	22.1	1734.1	13.6	0.10613	0.00080	0.31254	0.00448
Pod-26-9.1	309.4	115.5	0.38	71.3	0.00000	0.00000	0.0	1521.7	32.4	1499.5	19.8	0.09357	0.00098	0.26624	0.00634
Pod-30-1.1	70.4	55.7	0.81	17.8	0.00029	0.00004	0.5	1653.1	15.0	1651.7	21.0	0.10149	0.00116	0.29232	0.00300
Pod-30-10.	29.6	16.8	0.58	5.2	0.00106	0.00039	1.9	1198.9	19.2	1204.3	21.4	0.08029	0.00088	0.20439	0.00358
Pod-30-11.	86.3	49.9	0.59	12.8	0.00013	0.00012	0.2	1021.8	14.1	1003.9	39.6	0.07264	0.00144	0.17176	0.00257
Pod-30-12.	333.9	162.4	0.50	73.9	0.00007	0.00002	0.1	1468.6	7.8	1494.1	11.6	0.09331	0.00057	0.25585	0.00152
Pod-30-13.	145.4	72.7	0.51	22.2	−0.00001	0.00012	0.0	1049.6	8.4	1103.9	8.2	0.07633	0.00032	0.17682	0.00153
Pod-30-14.	348.4	176.2	0.52	84.9	0.00002	0.00003	0.0	1598.4	6.4	1627.5	6.4	0.10019	0.00035	0.28140	0.00127
Pod-30-15.	115.7	45.7	0.41	18.6	−0.00005	0.00003	−0.1	1098.3	18.6	1131.7	5.8	0.07740	0.00023	0.18575	0.00342
Pod-30-16.	290.3	393.4	1.39	40.3	0.00005	0.00004	0.1	959.5	8.7	982.3	6.2	0.07187	0.00022	0.16050	0.00158
Pod-30-17.	95.6	69.2	0.74	23.9	0.00008	0.00010	0.2	1637.1	10.4	1642.3	18.2	0.10098	0.00100	0.28912	0.00208
Pod-30-18.	118.5	40.0	0.35	27.6	−0.00003	0.00003	0.0	1533.9	11.6	1529.9	10.6	0.09510	0.00053	0.26864	0.00228
Pod-30-19.	167.3	117.6	0.72	46.7	0.00011	0.00000	0.2	1802.4	18.4	1697.9	10.4	0.10407	0.00059	0.32259	0.00376
Pod-30-2.1	48.0	32.5	0.69	25.2	0.00013	0.00008	0.2	3059.5	61.1	3059.7	6.8	0.23110	0.00098	0.60739	0.01518
Pod-30-20.	72.1	35.6	0.51	10.9	-0.00036	0.00014	−0.7	1036.1	13.4	1091.9	23.8	0.07588	0.00091	0.17435	0.00243
Pod-30-21.	90.1	64.9	0.74	23.0	0.00007	0.00008	0.1	1667.1	14.7	1651.7	17.8	0.10150	0.00098	0.29513	0.00294
Pod-30-21.	351.8	381.2	1.11	87.9	0.00002	0.00001	0.0	1635.1	6.4	1659.3	7.2	0.10191	0.00040	0.28872	0.00128
Pod-30-23.	192.0	137.8	0.74	47.9	0.00002	0.00002	0.0	1631.5	14.9	1674.3	5.4	0.10274	0.00031	0.28800	0.00298
Pod-30-24.	33.6	28.6	0.87	8.3	0.00018	0.00012	0.3	1621.2	35.4	1654.1	7.2	0.10163	0.00040	0.28595	0.00706
Pod-30-25.	22.0	12.6	0.59	3.9	0.00072	0.00055	1.3	1201.2	30.9	1288.1	32.6	0.08381	0.00142	0.20482	0.00576
Pod-30-26.	227.1	78.1	0.35	36.5	0.00004	0.00005	0.1	1098.6	5.5	1069.5	24.2	0.07504	0.00091	0.18581	0.00101
Pod-30-26.	83.9	73.7	0.90	12.6	0.00007	0.00018	0.1	1031.9	11.8	1006.7	9.0	0.07274	0.00033	0.17359	0.00214
Pod-30-27.	27.7	15.8	0.59	7.6	0.00022	0.00028	0.4	1784.1	5.2	1773.7	17.4	0.10846	0.00103	0.31885	0.00107
Pod-30-29.	28.2	34.6	1.26	4.0	0.00090	0.00032	1.6	984.8	26.9	1080.9	41.8	0.07546	0.00159	0.16505	0.00484
Pod-30-3.2	138.3	122.8	0.91	34.5	0.00008	0.00004	0.1	1632.0	12.9	1631.3	5.8	0.10039	0.00031	0.28809	0.00258

(*Continued*)

Table 2. (*Continued*)

Spot	U (ppm)	Th (ppm)	Th/U	^{206}Pb* (ppm)	^{204}Pb/^{206}Pb	±err	f_{206_4} (%)	^{206}Pb/^{238} U age	±err	^{207}Pb/^{206}Pb age	±err	^{207}Pb/^{206}Pb	±err	^{206}Pb/^{238} U	±err
Pod-30-30.	46.9	16.0	0.35	7.6	0.00021	0.00000	0.4	1112.2	17.9	1147.9	54.0	0.07804	0.00216	0.18831	0.00329
Pod-30-4.1	141.1	96.1	0.70	39.2	0.00011	0.00000	0.2	1793.6	15.1	1810.3	13.6	0.11066	0.00084	0.32079	0.00309
Pod-30-5.1	98.6	66.3	0.69	15.6	−0.00014	0.00009	−0.3	1083.2	23.8	1130.1	33.6	0.07734	0.00132	0.18298	0.00437
Pod-30-6.1	187.8	64.4	0.35	41.3	−0.00002	0.00001	0.0	1460.4	9.6	1527.9	6.6	0.09499	0.00034	0.25425	0.00186
Pod-30-7.1	40.7	29.1	0.73	6.3	−0.00018	0.00058	−0.3	1053.6	16.2	1054.1	15.8	0.07447	0.00058	0.17755	0.00295
Pod-30-8.1	155.7	165.4	1.09	39.4	0.00004	0.00006	0.1	1652.7	12.2	1685.9	4.8	0.10339	0.00028	0.29224	0.00245
Pod-30-9.1	91.8	77.1	0.86	13.4	0.00023	0.00000	0.4	1003.8	5.9	1019.3	6.2	0.07319	0.00023	0.16849	0.00106
Pod-10-10.	102.1	40.7	0.41	28.4	0.00012	0.00000	0.2	1799.5	13.1	1751.1	12.8	0.10712	0.00076	0.32201	0.00269
Pod-10-11.	293.7	192.9	0.67	77.2	0.00007	0.00002	0.1	1708.7	12.5	1676.5	10.2	0.10286	0.00058	0.30352	0.00253
Pod-10-12.	22.2	19.2	0.89	3.4	0.00018	0.00043	0.3	1040.1	16.1	962.9	41.2	0.07119	0.00146	0.17509	0.00293
Pod-10-12.	109.3	219.9	2.06	17.1	−0.00011	0.00007	−0.2	1072.6	36.5	985.7	41.0	0.07199	0.00147	0.18103	0.00666
Pod-10-14.	112.9	36.6	0.33	15.3	0.00022	0.00009	0.4	940.0	5.0	909.5	19.4	0.06936	0.00066	0.15698	0.00089
Pod-10-15.	124.0	135.6	1.12	37.2	0.00005	0.00002	0.1	1915.9	20.3	1878.7	10.0	0.11493	0.00064	0.34610	0.00424
Pod-10-16.	206.3	160.4	0.80	51.0	0.00004	0.00004	0.1	1620.5	17.8	1629.3	1.6	0.10028	0.00008	0.28580	0.00356
Pod-10-17.	117.2	76.9	0.67	29.0	0.00000	0.00000	0.0	1623.2	13.3	1613.9	10.6	0.09946	0.00057	0.28634	0.00266
Pod-10-17.	108.8	70.2	0.66	27.5	0.00006	0.00002	0.1	1653.1	26.0	1547.7	12.8	0.09600	0.00066	0.29232	0.00520
Pod-10-18.	281.2	66.7	0.24	69.4	0.00005	0.00002	0.1	1617.3	6.0	1618.3	4.4	0.09969	0.00023	0.28515	0.00119
Pod-10-19.	194.5	89.3	0.47	39.6	−0.00003	0.00003	−0.1	1362.5	31.3	1300.9	30.6	0.08436	0.00134	0.23535	0.00599
Pod-10-2.1	84.7	70.4	0.85	21.7	0.00003	0.00000	0.1	1669.0	12.3	1612.7	11.6	0.09939	0.00062	0.29550	0.00247
Pod-10-20.	130.7	79.2	0.62	32.7	−0.00002	0.00002	0.0	1637.2	16.0	1662.9	4.0	0.10212	0.00022	0.28914	0.00319
Pod-10-21.	75.8	66.0	0.89	19.3	0.00002	0.00001	0.0	1661.4	10.1	1630.7	10.0	0.10035	0.00055	0.29398	0.00202
Pod-10-22.	374.4	128.0	0.35	55.9	−0.00003	0.00001	−0.1	1026.0	7.3	1002.5	14.0	0.07259	0.00050	0.17251	0.00131
Pod-10-23.	225.8	211.9	0.96	53.6	0.00002	0.00003	0.0	1561.9	3.5	1633.1	2.2	0.10048	0.00012	0.27417	0.00070
Pod-10-24.	363.2	141.2	0.40	49.8	0.00006	0.00000	0.1	947.8	11.0	989.5	7.0	0.07213	0.00025	0.15838	0.00198
Pod-10-25.	412.3	139.4	0.35	101.5	0.00002	0.00002	0.0	1614.1	3.8	1605.5	2.2	0.09901	0.00011	0.28452	0.00075
Pod-10-26.	149.7	170.1	1.17	12.8	0.00005	0.00012	0.1	608.7	7.8	655.3	19.0	0.06146	0.00054	0.09902	0.00132
Pod-10-28.	266.1	81.5	0.31	41.3	0.00005	0.00001	0.1	1063.7	1.7	1042.9	4.8	0.07405	0.00018	0.17941	0.00033
Pod-10-29.	127.3	60.5	0.49	19.2	0.00004	0.00004	0.1	1037.3	9.0	1029.5	23.0	0.07356	0.00085	0.17457	0.00164
Pod-10-3.1	222.1	163.5	0.76	56.0	−0.00001	0.00001	0.0	1648.0	4.0	1663.3	5.6	0.10214	0.00031	0.29130	0.00080
Pod-10-30.	147.2	108.2	0.75	20.9	0.00006	0.00005	0.1	980.2	13.8	965.7	9.6	0.07129	0.00033	0.16422	0.00248
Pod-10-31.	95.7	44.9	0.48	20.3	0.00026	0.00001	0.5	1411.3	10.1	1434.5	6.4	0.09042	0.00030	0.24474	0.00194

(*Continued*)

https://doi.org/10.1017/S0016756819000384 Published online by Cambridge University Press

Table 2. (*Continued*)

Spot	U (ppm)	Th (ppm)	Th/U	$^{206}Pb^{*}$ (ppm)	$^{204}Pb/^{206}Pb$	±err	f_{206_4} (%)	$^{206}Pb/^{238}U$ age	±err	$^{207}Pb/^{206}Pb$ age	±err	$^{207}Pb/^{206}Pb$	±err	$^{206}Pb/^{238}U$	±err
Pod-10-4.1	28.9	4.9	0.17	8.4	0.00030	0.00009	0.5	1870.6	25.5	1852.9	17.2	0.11329	0.00108	0.33667	0.00528
Pod-10-2.1	84.7	70.4	0.85	21.7	0.00003	0.00000	0.1	1669.0	12.3	1612.7	11.6	0.09939	0.00062	0.29550	0.00247
Pod-10-20.	130.7	79.2	0.62	32.7	−0.00002	0.00002	0.0	1637.2	16.0	1662.9	4.0	0.10212	0.00022	0.28914	0.00319
Pod-10-21.	75.8	66.0	0.89	19.3	0.00002	0.00001	0.0	1661.4	10.1	1630.7	10.0	0.10035	0.00055	0.29398	0.00202
Pod-10-22.	374.4	128.0	0.35	55.9	−0.00003	0.00001	−0.1	1026.0	7.3	1002.5	14.0	0.07259	0.00050	0.17251	0.00131
Pod-10-23.	225.8	211.9	0.96	53.6	0.00002	0.00003	0.0	1561.9	3.5	1633.1	2.2	0.10048	0.00012	0.27417	0.00070
Pod-10-24.	363.2	141.2	0.40	49.8	0.00006	0.00000	0.1	947.8	11.0	989.5	7.0	0.07213	0.00025	0.15838	0.00198
Pod-10-25.	412.3	139.4	0.35	101.5	0.00002	0.00002	0.0	1614.1	3.8	1605.5	2.2	0.09901	0.00011	0.28452	0.00075
Pod-10-26.	149.7	170.1	1.17	12.8	0.00005	0.00012	0.1	608.7	7.8	655.3	19.0	0.06146	0.00054	0.09902	0.00132
Pod-10-28.	266.1	81.5	0.31	41.3	0.00005	0.00001	0.1	1063.7	1.7	1042.9	4.8	0.07405	0.00018	0.17941	0.00033
Pod-10-29.	127.3	60.5	0.49	19.2	0.00004	0.00004	0.1	1037.3	9.0	1029.5	23.0	0.07356	0.00085	0.17457	0.00164
Pod-10-3.1	222.1	163.5	0.76	56.0	−0.00001	0.00001	0.0	1648.0	4.0	1663.3	5.6	0.10214	0.00031	0.29130	0.00080
Pod-10-30.	147.2	108.2	0.75	20.9	0.00006	0.00005	0.1	980.2	13.8	965.7	9.6	0.07129	0.00033	0.16422	0.00248
Pod-10-31.	95.7	44.9	0.48	20.3	0.00026	0.00001	0.5	1411.3	10.1	1434.5	6.4	0.09042	0.00030	0.24474	0.00194
Pod-10-4.1	28.9	4.9	0.17	8.4	0.00030	0.00009	0.5	1870.6	25.5	1852.9	17.2	0.11329	0.00108	0.33667	0.00528
Pod-10-5.1	113.0	59.3	0.54	23.4	0.00007	0.00003	0.1	1382.5	15.7	1336.3	18.8	0.08591	0.00085	0.23919	0.00301
Pod-10-6.1	80.5	60.1	0.77	23.4	0.00001	0.00008	0.0	1868.9	18.9	1867.1	12.6	0.11418	0.00080	0.33630	0.00390
Pod-10-7.1	147.4	87.4	0.61	33.3	−0.00002	0.00003	0.0	1495.9	14.6	1460.7	15.4	0.09168	0.00074	0.26118	0.00285
Pod-10-8.1	228.6	69.3	0.31	57.3	−0.00003	0.00001	−0.1	1640.3	9.2	1599.5	9.4	0.09869	0.00050	0.28975	0.00184
U-1.1	71.7	38.2	0.55	12.7	−0.00006	0.00013	−0.1	1198.7	23.1	1164.9	36.8	0.07871	0.00148	0.20435	0.00430
U-10.1	370.3	109.1	0.30	61.0	0.00026	0.00003	0.5	1122.6	7.0	1174.7	5.6	0.07910	0.00022	0.19022	0.00129
U-11.1	107.7	41.7	0.40	18.9	0.00000	0.00000	0.0	1190.1	1.8	1131.3	1.4	0.07739	0.00006	0.20276	0.00034
U-12.1	135.3	62.2	0.47	23.8	−0.00005	0.00005	−0.1	1191.8	7.9	1139.1	8.2	0.07770	0.00032	0.20307	0.00147
U-13.1	159.0	12.9	0.08	24.8	0.00015	0.00003	0.3	1069.2	4.7	1048.7	32.0	0.07426	0.00119	0.18040	0.00087
U-14.1	179.4	37.6	0.22	27.8	0.00004	0.00008	0.1	1061.2	13.1	1053.9	34.6	0.07446	0.00129	0.17895	0.00240
U-15.1	285.7	280.7	1.01	64.7	0.00003	0.00003	0.1	1498.9	10.3	1457.1	3.0	0.09150	0.00014	0.26178	0.00202
U-17.1	251.9	144.3	0.59	62.6	0.00006	0.00002	0.1	1626.4	4.7	1626.9	14.4	0.10015	0.00077	0.28697	0.00094
U-18.1	128.8	152.5	1.21	20.2	−0.00002	0.00006	0.0	1075.3	9.3	1049.5	25.6	0.07429	0.00095	0.18152	0.00170
U-19.1	278.0	242.2	0.89	122.1	0.00001	0.00001	0.0	2646.0	17.1	2695.3	5.8	0.18466	0.00067	0.50751	0.00400
U-2.1	109.4	91.1	0.85	27.0	0.00000	0.00000	0.0	1614.4	19.6	1625.5	9.2	0.10008	0.00049	0.28458	0.00390
U-21.1	57.4	48.7	0.87	12.8	0.00012	0.00013	0.2	1477.6	16.1	1442.9	19.4	0.09083	0.00093	0.25761	0.00315

(*Continued*)

Table 2. (*Continued*)

Spot	U (ppm)	Th (ppm)	Th/U	$^{206}Pb^*$ (ppm)	$^{204}Pb/^{206}Pb$	±err	f_{206_4} (%)	$^{206}Pb/^{238}U$ age	±err	$^{207}Pb/^{206}Pb$ age	±err	$^{207}Pb/^{206}Pb$	±err	$^{206}Pb/^{238}U$	±err
U-22.1	84.3	46.7	0.57	31.8	0.00001	0.00002	0.0	2334.4	11.9	2306.1	3.6	0.14655	0.00032	0.43637	0.00264
U-23.2	148.4	59.0	0.41	25.4	0.00003	0.00004	0.1	1162.8	14.7	1131.7	18.0	0.07741	0.00070	0.19768	0.00274
U-24.1	131.3	80.5	0.63	33.7	0.00005	0.00004	0.1	1673.6	12.5	1653.1	7.8	0.10157	0.00044	0.29643	0.00252
U-26.1	299.0	301.8	1.04	75.9	0.00034	0.00004	0.6	1658.3	1.8	1612.5	3.6	0.09937	0.00020	0.29335	0.00036
U-27.1	76.6	86.7	1.16	19.4	0.00019	0.00002	0.3	1658.0	5.8	1579.9	10.6	0.09766	0.00056	0.29331	0.00117
U-28.1	107.9	28.4	0.27	22.1	−0.00010	0.00006	−0.2	1372.2	18.8	1318.1	16.8	0.08511	0.00075	0.23721	0.00360
U-29.1	144.5	62.6	0.44	22.1	0.00002	0.00006	0.0	1047.1	8.3	1008.9	15.4	0.07282	0.00056	0.17636	0.00151
U-3.1	179.3	175.6	1.00	42.9	−0.00001	0.00002	0.0	1572.5	14.1	1617.7	11.8	0.09965	0.00064	0.27627	0.00280
U-30.1	76.9	50.1	0.67	19.1	0.00017	0.00002	0.3	1624.0	15.9	1588.9	5.4	0.09813	0.00028	0.28650	0.00318
U-31.1	82.1	64.3	0.80	20.5	0.00013	0.00004	0.2	1635.7	11.7	1606.9	3.4	0.09908	0.00019	0.28883	0.00234
U-33.1	65.8	43.4	0.68	22.7	0.00008	0.00005	0.2	2166.4	8.6	2097.3	5.4	0.12994	0.00040	0.39944	0.00187
U-34.1	388.4	149.9	0.40	71.0	0.00007	0.00002	0.1	1234.7	6.1	1316.5	6.2	0.08504	0.00028	0.21110	0.00114
U-37.2	217.0	91.5	0.43	43.3	0.00009	0.00005	0.2	1336.7	52.4	1429.5	36.2	0.09019	0.00174	0.23041	0.00996
U-38.1	89.0	50.0	0.58	32.1	0.00000	0.00000	0.0	2245.5	25.5	2346.9	10.2	0.15009	0.00089	0.41670	0.00560
U-38.2	279.5	167.9	0.62	74.3	0.00008	0.00001	0.1	1727.4	3.4	1758.5	6.8	0.10756	0.00040	0.30729	0.00067
U-4.1	95.9	80.0	0.86	26.2	0.00006	0.00004	0.1	1771.0	1.6	1784.7	14.4	0.10912	0.00086	0.31617	0.00032
U-40.1	157.3	79.2	0.52	24.4	0.00014	0.00000	0.2	1061.7	5.7	1110.1	12.6	0.07657	0.00048	0.17903	0.00104
U-5.1	265.9	45.9	0.18	39.0	0.00013	0.00003	0.2	1008.2	4.0	981.3	7.0	0.07184	0.00025	0.16929	0.00073
U-7.1	124.7	62.5	0.51	34.9	0.00001	0.00007	0.0	1806.6	15.0	1772.5	8.8	0.10839	0.00053	0.32346	0.00308
U-8.1	149.8	71.9	0.49	35.1	0.00021	0.00005	0.4	1545.8	9.8	1485.5	13.6	0.09288	0.00068	0.27098	0.00193
U-8.2	339.9	175.4	0.53	85.8	0.00003	0.00001	0.1	1650.2	11.9	1648.5	9.2	0.10133	0.00050	0.29174	0.00237
U-9.1	213.7	84.5	0.41	47.3	0.00004	0.00005	0.1	1467.9	6.0	1450.9	8.6	0.09121	0.00042	0.25571	0.00117

Errors are 1-sigma; Pb_c and Pb* indicate the common and radiogenic portions, respectively.
Error in standard calibration was 0.14 %.

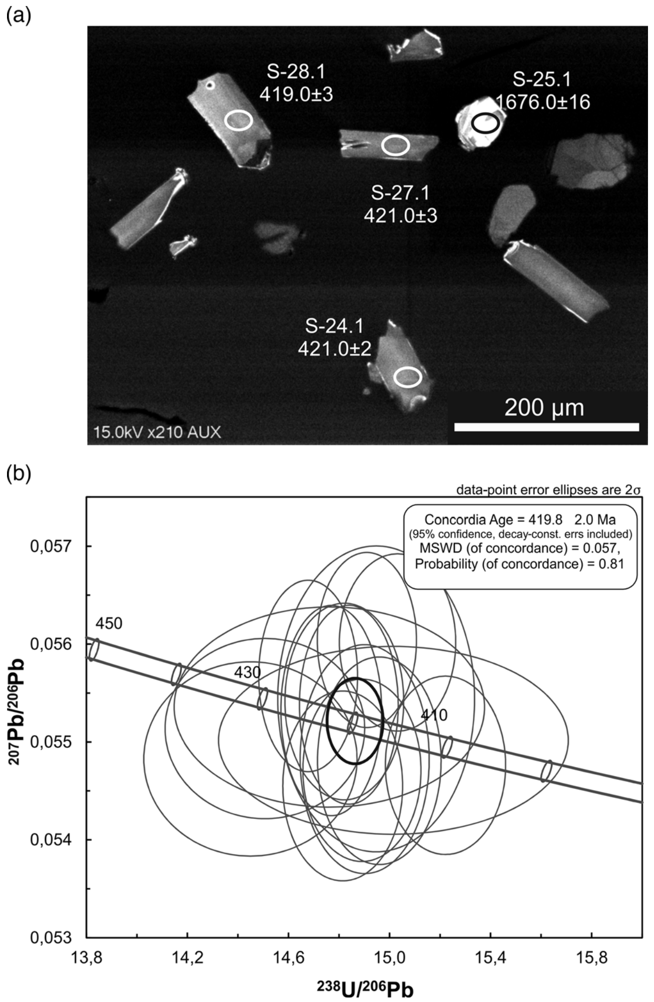

Fig. 4. (a) Representative CL images of zircon crystals from the diorite in the Sosnowiec IG-1 borehole with location of analysed spots and obtained isotope ages. (b) Results of U–Pb isotope studies of magmatic zircons from the Sosnowiec diorite presented as a concordia plot.

a wide spectrum of concordant ages (Fig. 5b). Most of them are enclosed between 1 and 1.8 Ga where the two intervals of highest frequency (*c*. 1–1.2 Ga and 1.4–1.8 Ga) can be observed (Fig. 5c). Evidently, younger and older ages were defined for single crystals only. They correspond to *c*. 0.4, 0.6, 2.2, 2.6 and 3 Ga.

5. Discussion

The U–Pb age for zircons from the diorite, and results of earlier age estimation of the Bardo diabase (Nawrocki *et al.* 2013), clearly indicate that these magmatic bodies were emplaced at approximately the same time, i.e. close to the Silurian/Devonian boundary. These intrusions point to extensional processes at the Silurian/Devonian boundary (Krzemiński, 2004) common for both the BVT and the MT which must have been situated close to each other at least since the latest Silurian, forming the marginal part of the Old Red Continent. The geochemical features of both intrusions are generally similar (Krzemiński, 2004). They display a negative Nb anomaly. This can indicate a contribution of a 'subduction component' in the source or crustal contamination (e.g. Pin & Marini, 1993). However, assimilation of crustal material did not occur on a large scale, as manifested by low large-ion lithopile elements and SiO_2 contents (Krzemiński, 2004). Because of this, the negative Nb anomaly arose in these rocks most probably during subduction. This 'subduction component' was primarily interpreted as having originated in the lithospheric mantle due to late Proterozoic subduction of the Tornquist Sea under the Gondwana active margin (Krzemiński, 2004). In some parts of the MT, the Silurian/Devonian tectonic activity is documented by coarse-grained deposits. After the early Ludlow and before the 'old red' type (Pragian? – Emsian) sedimentation, the Łapczyca, Miedziana Góra and Gruchawka conglomerates (Fig. 6) were deposited close to the zones of the main dislocations that separate the MT from the BVT and from the Łysogóry terrane (Kowalski, 1983; Buła, 2000; Malec, 2001). Clastic rocks of the Łapczyca Formation were tectonically deformed and tilted up to 60°, which is significantly more than for overlying rocks (Buła, 2000). A tectonic discordance between Silurian and Emsian strata also occurs at the NE margin of the MT (Kowalczewski & Lisik, 1974).

Lack of Lower Devonian zircons and phenocrysts of quartz in tuffs from Ujazd and Podłazie indicates derivation most probably from a mafic type of volcanic source. The age spectrum of detrital zircons from these localities points to their Baltic (Sveconorwegian and Transscandinavian) derivation, with the two characteristic frequency peaks at *c*. 1 Ga and 1.6 Ga (see e.g. Zeh & Gerdes, 2010; Willner *et al.* 2013). Neoproterozoic and early Palaeozoic ages were only found in two single grains from the Podłazie section (Fig. 5c; Table 2). The tuffs could not be derived from the neighbouring part of Baltica since Emsian volcanic activity has not been documented in that area. The zircons from the Podłazie and Ujazd sections were most probably derived from the Rheno-Hercynian Zone (RHZ) where bimodal volcanism is documented. According to Zeh & Gerdes (2010), part of the RHZ with the Avalonian basement was covered by detritus derived from Baltica in the Early Devonian. Zircons from these sediments and the Avalonian basement were reworked during volcanic eruptions producing tuffs that were deposited in the area of the Holy Cross Mountains. Given the quite large size of these zircons, the distance of their air transportation was most probably not longer than 1000 km (see e.g. Stevenson *et al.* 2015).

The geochronological data obtained can be considered in terms of the tectonic evolution of post-Caledonian Europe. They fit well with the tectonic models by Kroner *et al.* (2007) and Franke *et al.* (2017) that are shown in Figure 7. Magmatic intrusions emplaced close to the Silurian/Devonian boundary in the area of the BVT and MT were associated with extensional processes that must have been linked temporally and spatially with the closure of the Rheic Ocean and simultaneous opening of the Rheno-Hercynian Basin, and finally the Rheno-Hercynian Ocean. However, the extension that affected the BVT and MT was too weak to open an oceanic basin. This extensional event was followed by short-lived sinistral transpression (Żaba, 1999) and most probably translation in a southeastward direction of the BVT and MT (see Kozłowski *et al.* 2014). Further extension in this area (Żaba, 1999) and in the Rheno-Hercynian Basin, with its peak in the Emsian (Oncken *et al.* 1999), was accompanied by the bimodal volcanic activity (Penfound-Marks & Shail, 2015) which caused tuff sedimentation in the Emsian of the Holy Cross Mountains. Since both tectonic blocks were close to an early Variscan subduction zone (Kroner *et al.* 2007), the negative Nb anomaly noted in the mafic rocks from the BVT and MT (Krzemiński, 2004) might have been a consequence of Palaeozoic subduction of the Rheic Ocean. According to the reconstruction of Franke *et al.* (2017), the Sosnowiec diorite and the Bardo diabase could be linked with the back-arc extension proposed *c*. 425–410 Ma ago in the marginal (Avalonian) part of

https://doi.org/10.1017/S0016756819000384 Published online by Cambridge University Press

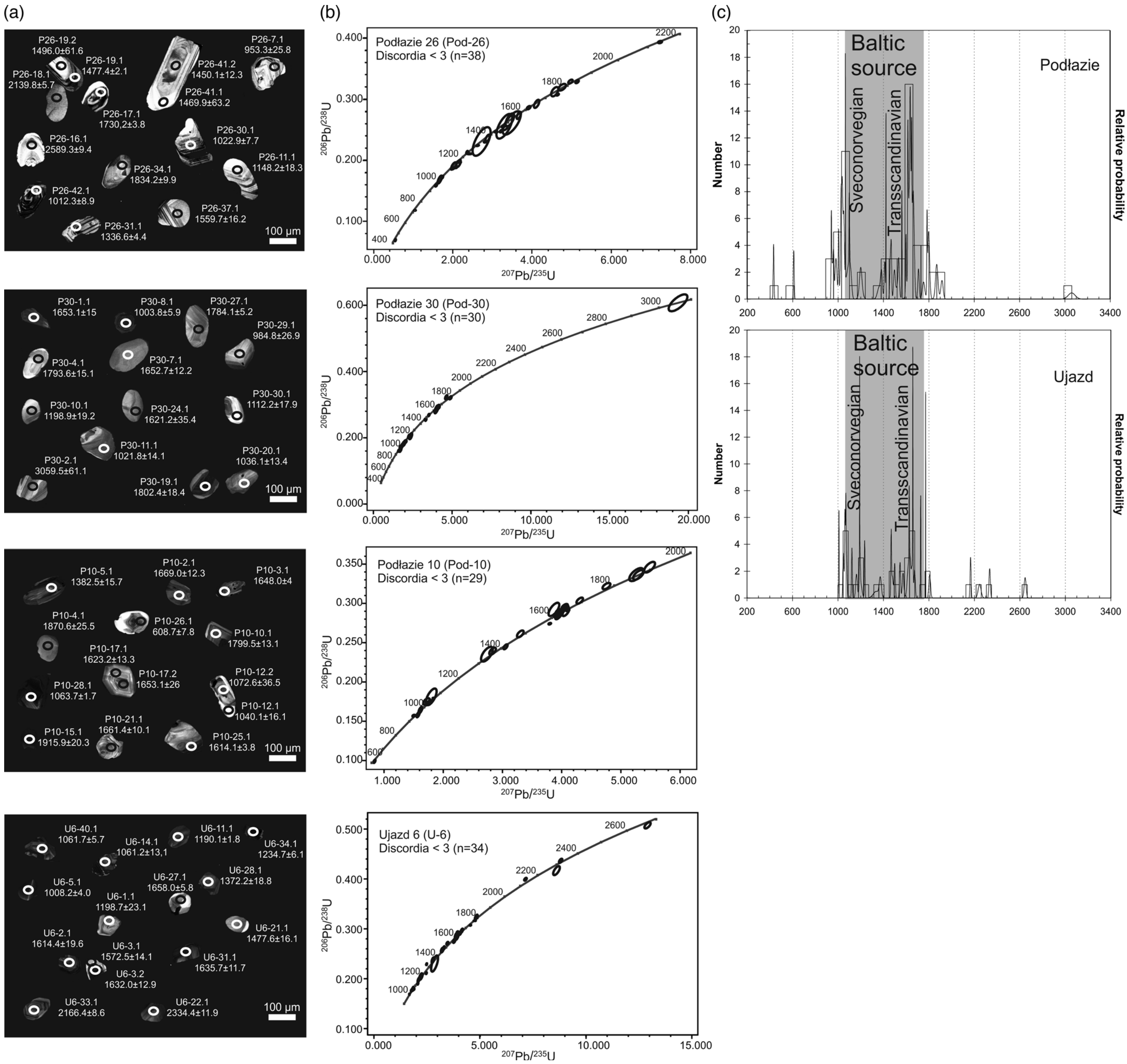

Fig. 5. (a) Representative CL images of zircon crystals from Emsian tuffs sampled in Podłazie and Ujazd with location of the analysed spots and obtained isotope ages. (b) Results of U–Pb isotope studies of detrital zircons from Podłazie and Ujazd shown as concordia plots. (c) Probability density diagrams of U–Pb ages of detrital zircons from Podłazie and Ujazd.

the Old Red Continent (Fig. 7b). These intrusions cannot be directly connected with the opening of the Rheno-Hercynian Ocean that started in the Emsian (Franke *et al.* 2017), i.e. at least 12 Ma later than the emplacement of intrusions within the BVT and MT.

6. Conclusions

The U–Pb age of diorite intrusion (420 ± 2 Ma) from the northern part of the BVT is comparable with the combined Ar–Ar and magnetostratigraphic age of the Bardo diabase intrusion (425–417 Ma) from the northern part of the MT. These intrusions were emplaced during the same event of regional tectonic extension at the Silurian/Devonian boundary. This event was most probably associated with the Rheic Ocean closure in this part of Europe already proposed by S Hoenig (unpub. PhD thesis, Masaryk Univ., Brno, 2016) and with the onset of extension forming the Rheno-Hercynian Basin. The tectonic extension in the BVT and MT was too weak to open an oceanic domain. The negative Nb anomaly characteristic of both intrusions could be linked with Palaeozoic subduction of the Rheic Ocean under the SE margin of the Old Red Continent. Traces of younger, i.e. Emsian, magmatic activity in the Rheno-Hercynian Basin were recorded in the northern part of the MT where several horizons of tuffaceous horizons occur within the clastic rocks of this age. Volcanic ashes were transported to the MT from the Rheno-Hercynian domain,

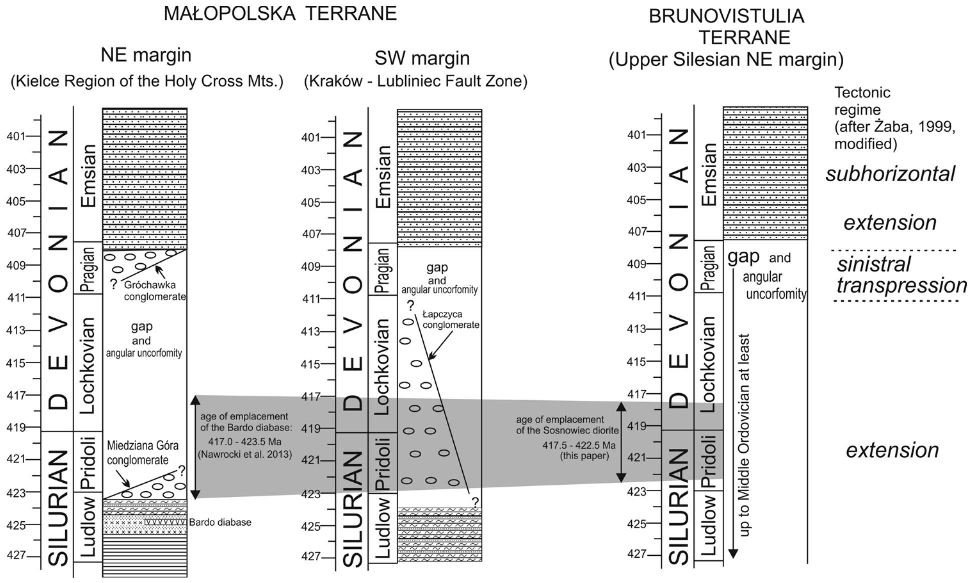

Fig. 6. Stratigraphy around the Silurian/Devonian boundary in the marginal parts of the Małopolska and Brunovistulia terranes. Stratigraphic positions of mafic intrusions from both terranes are marked by the grey belt. Changes of tectonic regime (Żaba, 1999) are also shown.

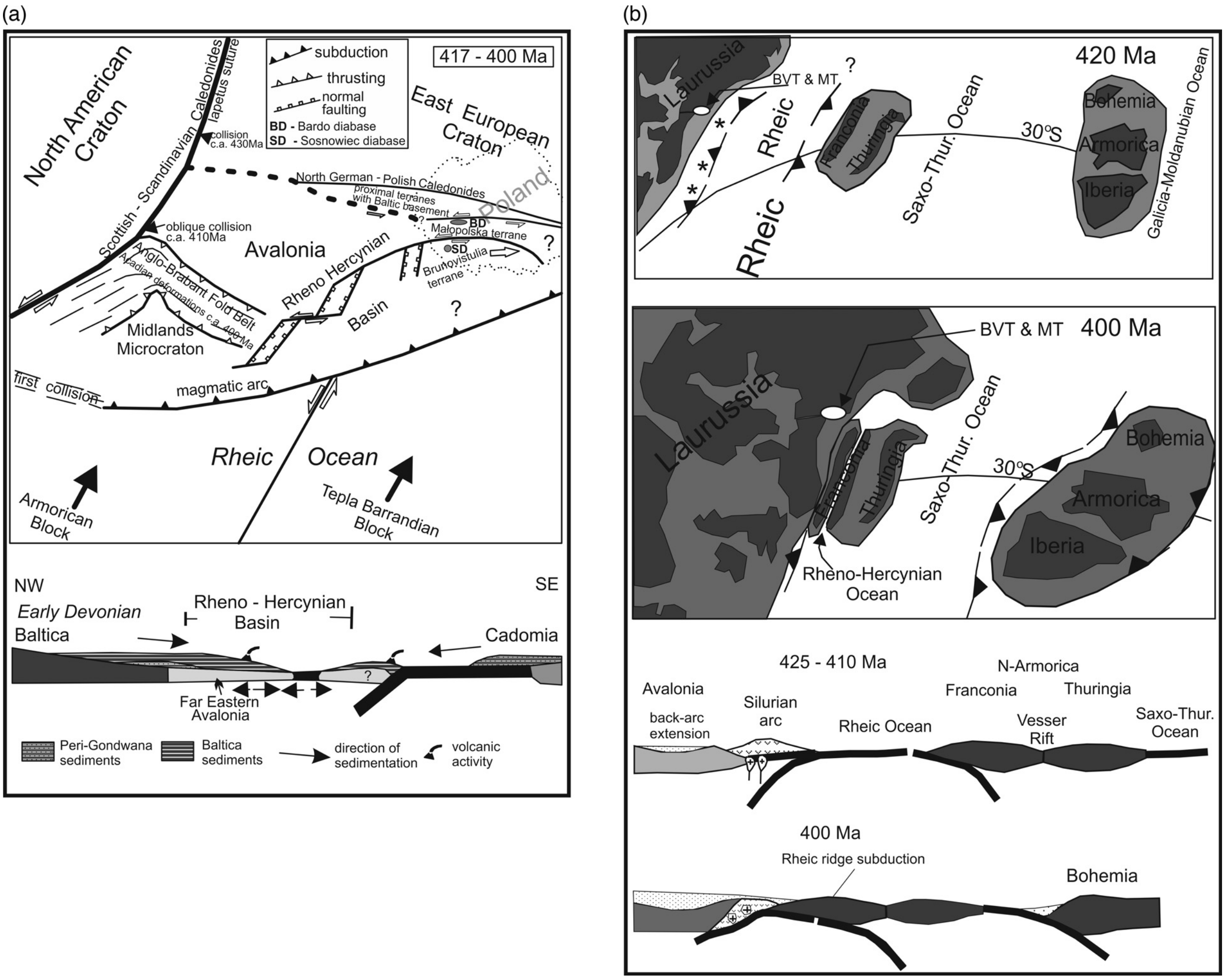

Fig. 7. (a) Onset of oblique subduction and collision processes along the European segment of the Rheic suture (schematic map modified after Kroner *et al.* 2007) and simplified geotectonic cross-section (lower part of figure) through the German part of the Reno-Hercynian Basin in the Lower Devonian (slightly modified after Zeh & Gerdes, 2010). (b) Late Silurian and Early Devonian palaeogeography of the European part of the Rheic Ocean and the cross-sections (lower part of figure) illustrating the plate-tectonic evolution in the central European segment of the Variscides during Late Silurian to Early Devonian (after Franke *et al.* 2017; simplified). BVT – Brunosilesia Terrane, MT – Małopolska Terrane, BD – Bardo diabase, SD – Sosnowiec diorite.

https://doi.org/10.1017/S0016756819000384 Published online by Cambridge University Press

where the eruptions most probably had a mafic composition. The magma assimilated detrital zircons from a sedimentary succession of Baltica provenance that was derived from western and central Scandinavia and laid down at the margin of the Rheno-Hercynian Ocean.

Author ORCIDs. Jerzy Nawrocki, 0000-0002-9644-0224; Piotr Szrek, 0000-0001-9855-2003

Acknowledgements. Financial support for this study was provided by the Polish Geological Institute – NRI. We are grateful to Mark Hounslow (Lancaster University) for substantial improvement of the English of the manuscript. Three anonymous reviewers, Prof. Christian Pin and Prof. Ulf Linnemann are thanked for valuable remarks. We also thank Prof. Ian Williams for discussion of our U–Pb data and Paweł Derkowski for help in BSE imaging.

References

Belka Z, Valverde-Vaquero P, Dörr W, Ahrendt H, Wemmer K, Franke W and Schäfer J (2002) Accretion of first Gondwana-derived terranes at the margin of Baltica. In *Paleozoic Amalgamation of Central Europe* (eds JA Winchester, TC Pharaoh and J Verniers), pp. 19–36. Geological Society of London, Special Publication no. 201.

Bogacz W and Krokowski J (1981) Rotation of the basement of the Upper Silesian Coal Basin. *Annales Societatis Geologorum Poloniae* **51**, 361–81.

Buła Z (2000) Lower Palaeozoic of Upper Silesia and West Małopolska. *Prace Państwowego Instytutu Geologicznego* **171**, 1–89 (in Polish with English summary).

Czarnocki J (1938) *Ogólna mapa geologiczna Polski w skali 1:100 000. Arkusz Kielce*. Warszawa: Państwowy Instytut Geologiczny.

Dadlez R (1995) Debates about pre-Variscan tectonics of Poland. *Studia Geophysica et Geodætica* **39**, 227–34.

Dudek A (1980) The crystalline basement block of the outer Carpathians in Moravia: Bruno-Vistulicum. *Rozprawy Československe Akademie Ved* **90**, 81–5.

Fatka O and Vavrdova M (1998) Early Cambrian Acritarcha from sediments underlaying the Devonian in Moravia (Menin-1 borehole, southern Moravia). *Bulletin of Czech Geological Survey* **73**, 55–60.

Fijałkowska-Mader A and Malec J (2011) Biostratigraphy of the Emsian to Eifelian in the Holy Cross Mountains (Poland). *Geological Quarterly* **55**, 109–38.

Franke W, Cocks LRM and Torsvik TH (2017) The Palaeozoic Variscan oceans revisited. *Gondwana Research* **48**, 257–84.

Friedl G, Fritz A, Von Quadt A, McNaughton NJ and Fletcher IR (2001) Results of conventional and SHRIMP U-Pb zircon dating in the south-eastern Bohemian Massif (Austria, Czech Republic): implications for a delineation of different Peri-Gondwana terranes in Variscan Central Europe. *ESF EUROPROBE Meeting 'Neoproterozoic–Early Palaeozoic Time-Slice Symposium: Orogeny and Cratonic Response on the Margins of Baltica', Ankara, Abstracts*, pp. 16–18.

Gradstein FM, Ogg JG, Schmitz MD and Ogg GM (2012) *The Geologic Time Scale 2012*. Elsevier.

Hegner E and Kröner A (2000) Review of Nd isotopic data and xenocrystic and detrital zircon ages from the pre-Variscan basement in the eastern Bohemian Massif: speculations on palinspastic reconstructions. In *Orogenic Processes, Quantification and Modelling in the Variscan Belt* (eds W Franke, V Haak, O Oncken and D Tanner), pp. 113–30. Geological Society of London, Special Publication no. 179.

Kalvoda J, Babek O, Fatka O, Leichmann J, Melichar R, Nehyba S and Spacek P (2008) Brunovistulian terrane (Bohemian Massif, Central Europe) from late Proterozoic to late Paleozoic: a review. *International Journal of Earth Sciences* **97**, 497–518.

Kowalczewski Z and Lisik R (1974) Nowe dane o diabazach i budowie geologicznej Prągowca w Górach Świętokrzyskich. *Biuletyn Instytutu Geologicznego* **275**, 113–52.

Kowalski WR (1983) Stratigraphy of the Upper Precambrian and lowest Cambrian strata in southern Poland. *Acta Geologica Polonica* **33**, 183–218.

Kozłowski W, Domańska-Siuda J and Nawrocki J (2014) Geochemistry and petrology of the Upper Silurian greywackes from the Holy Cross Mountains (central Poland): implications for the Caledonian history of the southern part of the Trans-European Suture Zone (TESZ). *Geological Quarterly* **58**, 311–36.

Kroner U, Hahn T, Romer RL and Linnemann U (2007) The Variscan orogeny in the Saxo-Thuringian zone – heterogeneous overprint of Cadomian/Paleozoic Peri-Gondwana crust. In *The Evolution of the Rheic Ocean: From Avalonian-Cadomian Active Margin to Alleghenian-Variscan Collision* (eds U Linnemann, RD Nance, P Kraft and G Zulauf), pp. 153–72. Geological Society of America, Special Paper no. 423.

Krzemiński L (2004) Geochemical constraints on the origin of the mid-Paleozoic diabases from the Holy Cross Mts. and Upper Silesia, southeastern Poland. *Geological Quarterly* **48**, 147–58.

Kusiak M, Kędzior A, Paszkowski M, Suzuki K, Gonzalez-Alvarez I, Wajsprych B and Doktor M (2006) Provenance implications of Th-U-Pb electron microprobe ages from detrital monazite in the Carboniferous Upper Silesia Coal Basin, Poland. *Lithos* **88**, 56–71.

Leichman J and Höck V (2001) The Brunovistulicum: a Gondwana derived terrain accreted to Baltica. *ESF EUROPROBE Meeting, 'Neoproterozoic–Early Palaeozoic Time-Slice Symposium: Orogeny and Cratonic Response on the Margins of Baltica', Ankara, Abstracts*, pp. 37–8.

Linnemann U, Herbosch A, Liégeois JP, Pin CH, Gärtner A and Hofmann M (2012) The Cambrian to Devonian odyssey of the Brabant Massif within Avalonia: a review with new zircon ages, geochemistry, Sm-Nd isotopes, stratigraphy and palaeogeography. *Earth-Science Reviews* **112**, 126–54.

Ludwig KR (2000) *SQUID 1.00, A User's Manual*. Berkeley, California: Berkeley Geochronology Center, Special Publication no. 2.

Ludwig KR (2003) Isoplot/Ex version 3.0. *A Geochronological Toolkit for Microsoft Excel*. Berkeley, California: Berkeley Geochronology Center, Special Publication no. 1a.

Malec J (2001) Sedimentology of deposits from around the Caledonian unconformity in the western Holy Cross Mts. *Geological Quarterly* **45**, 397–415.

Malinowski M, Żelaźniewicz A, Grad M, Guterch A and Janik T (2005) Seismic and geological structure of the crust in the transition from Baltica to Palaeozoic Europe in SE Poland – CELEBRATION 2000 experiment, profile CEL02. *Tectonophysics* **401**, 55–77.

Mazur S, Kröner A and Szczepański J (2010) Single zircon U-Pb ages and geochemistry of granitoid gneisses from SW Poland: evidence for an Avalonian affinity of the Brunian microcontinent. *Geological Magazine* **147**, 508–26.

Moczydłowska M (1997) Proterozoic and Cambrian successions in Upper Silesia: an Avalonian terrane in Southern Poland. *Geological Magazine* **134**, 679–89.

Nawrocki J (2000) Late Silurian paleomagnetic pole from the Holy Cross Mountains: constraints for the post-Caledonian tectonic activity of the Trans-European Suture Zone. *Earth and Planetary Science Letters* **179**, 325–34.

Nawrocki J (2015) Once again about terranes in Poland and their wandering. *Przegląd Geologiczny* **63**, 1272–83 (in Polish with English summary).

Nawrocki J, Krzemiński L and Pańczyk M (2010) ^{40}Ar-^{39}Ar ages of selected rocks and minerals from the Kraków–Lubliniec Fault Zone, and their relation to the Paleozoic structural evolution of the Małopolska and Brunovistulian terranes (S Poland). *Geological Quarterly* **54**, 289–300.

Nawrocki J and Poprawa P (2006) Development of Trans-European Suture Zone in Poland: from Ediacaran rifting to Early Palaeozoic accretion. *Geological Quarterly* **50**, 59–76.

Nawrocki J, Salwa S and Pańczyk M (2013) New ^{40}Ar-^{39}Ar age constraints for magmatic and hydrothermal activity in the Holy Cross Mts. (southern Poland). *Geological Quarterly*, **57**, 551–60.

Nawrocki J, Żylińska A, Buła Z, Grabowski J, Krzywiec P and Poprawa P (2004) Early Cambrian location and affinities of the Brunovistulian terrane (Central Europe) in the light of palaeomagnetic data. *Journal of the Geological Society of London* **161**, 513–22.

Oncken O, von Winterfeld C and Dittmar U (1999) Accretion and inversion of rifted passive margin – the Late Palaeozoic Rhenohercynian fold and thrust belt. *Tectonics* **18**, 75–91.

Pajchlowa M and Miłaczewski L (1974) Dewon dolny. In: *Atlas litologiczno-paleogeograficzny obszarów platformowych Polski. Cz. I – Proterozoik i paleozoik* (eds J Czermiński and M Pajchlowa). Warszawa: Wydawnictwa Geologiczne.

Penfound-Marks LRG and Shail RK (2015) Early Devonian rift-related felsic igneous rocks in the western Looe Basin, South-West England. *Geoscience in South-West England* **13**, 471–82.

Pin C and Marini F (1993) Early Ordovician continental break-up in Variscan Europe: Nd-Sr isotope and trace element evidence from bimodal igneous associations of the southern Massif Central, France. *Lithos* **29**, 177–96.

Přichystal A (1999) K-Ar age determination of basaltic dyke from Zelesice (Brno massif). *Geologické výzkumy na Moravă ve Slezsku* **6**, 120–1.

Shatz M, Zwing A, Tait J, Belka Z, Soffel HC and Bachtadse V (2006) Paleomagnetism of Ordovician carbonate rocks from Małopolska Massif, Holy Cross Mountains, SE Poland – magnetostratigraphic and geotectonic implications. *Earth Planetary and Science Letters* **244**, 349–60.

Słaby E, Breitkreuz C, Żaba J, Domańska-Siuda J, Gaidzik K, Falenty K and Falenty A (2010) Magma generation in an alternating transpressional-transtensional regime, the Kraków-Lubliniec Fault Zone, Poland. *Lithos* **119**, 251–68.

Steiger RH and Jäger E (1977) Subcommission on geochronology: convention on the use of decay constants in geo- and cosmochronology. *Earth and Planetary Science Letters* **36**, 359–62.

Stevenson JA, Millington SC, Beckett FM, Swindles GT and Thordarson T (2015) Big grains go far: understanding the discrepancy between tephrochronology and satellite infrared measurements of volcanic ash. *Atmospheric Measurement Techniques* **8**, 2069–91.

Szulczewski M and Porębski S (2008) Stop 1 – Bukowa Góra, Lower Devonian. In *Ichnological Sites of Poland. The Holy Cross Mountains and the Carpathian Flysch. The Second International Congress on Ichnology. Cracow, Poland, August 2 – September 8, 2008. The Pre-Congress and Post-Congress Field Trip Guidebook* (eds G Pieńkowski and A Uchman), pp. 18–37. Warsaw: Polish Geological Institute.

Szrek P and Dupret V (2017) Placoderms in the Lower Devonian 'placoderm sandstone' of the Holy Cross Mountains, Poland with biostratigraphical and palaeogeographical implications. *Acta Palaeontologica Polonica* **62**, 789–800.

Tarnowska M (1976) Lithological correlation of Lower Devonian in the eastern part of the Holy Cross Mountains. *Biuletyn Instytutu Geologicznego* **296**, 75–115 (in Polish with English summary).

Tera F and Wasserburg GJ (1972) U-Th-Pb systematics in three Apollo 14 basalts and the problem of initial Pb in lunar rocks. *Earth and Planetary Science Letters* **14**, 281–304.

Unrug R, Harańczyk C and Chocyk-Jamińska M (1999) Easternmost Avalonian and Armorican-Cadomian terranes of central Europe and Caledonian-Variscan evolution of the polydeformed Kraków mobile belt: geological constraints. *Tectonophysics* **302**, 133–57.

Walczak A and Bełka Z (2017) Fingerprinting Gondwana versus Baltica provenance: Na and Sr isotopes in Lower Paleozoic clastic rocks of the Małopolska and Łysogóry terranes, southern Poland. *Gondwana Research* **45**, 138–51.

Williams IS (1998) U-Th-Pb geochronology by ion microprobe. In *Applications of Microanalytical Techniques to Understanding Mineralizing Processes* (eds MA McKibben, WC Shanks III and WI Ridley), pp. 1–35. Reviews in Economic Geology, vol. **7**.

Williams IS and Claesson S (1987) Isotopic evidence for the Precambrian provenance and Caledonian metamorphism of high grade paragneisses from the Seve Nappes, Scandinavian Caledonides: II Ion microprobe zircon U-Th-Pb. *Contributions to Mineralogy and Petrology* **97**, 205–17.

Willner AP, Barr S, Gerdes A, Massonne HJ and White C (2013) Origin and evolution of Avalonia: evidence from U-Pb and Lu-Hf isotopes in zircon from the Mira terrane, Canada, and the Stavelot Massif, Belgium. *Journal of the Geological Society of London* **170**, 769–84.

Winchester JA and The Pace TMR Networkteam (2002) Paleozoic amalgamation of Central Europe: new results from recent geological and geophysical investigations. *Tectonophysics* **360**, 5–21.

Wójcik K (2015) The uppermost Emsian and lower Eifelian in the Kielce Region of the Holy Cross Mts. Part I: Lithostratigraphy. *Acta Geologica Polonica* **65**, 141–79.

Żaba J (1999) The structural evolution of Lower Palaeozoic succession in the Upper Silesia Block and Małopolska Block border zone (Southern Poland). *Prace Państwowego Instytutu Geologicznego* **166**, 1–162 (in Polish with English summary).

Zeh A and Gerdes A (2010) Baltica- and Gondwana-derived sediments in the Mid-German Crystalline Rise (Central Europe): implications for the closure of the Rheic ocean. *Gondwana Research* **17**, 254–63.

Żelaźniewicz A, Buła Z, Fanning M, Seghedi A and Żaba J (2009) More evidence on Neoproterozoic terranes in Southern Poland and southeastern Romania. *Geological Quarterly* **53**, 93–124.

Żelaźniewicz A, Pańczyk M, Nawrocki J and Fanning M (2008) A Carboniferous/Permian, calc-alkaline, I-type granodiorite from the Małopolska Block, Southern Poland: implications from geochemical and U-Pb zircon age data. *Geological Quarterly* **52**, 301–8.

Żylińska A (2002) Stratigraphic and biogeographic significance of Late Cambrian trilobites from Lysogóry (Holy Cross Mountains, central Poland). *Acta Geologica Polonica* **52**, 217–38.

https://doi.org/10.1017/S0016756819000384 Published online by Cambridge University Press